Phys. Lett. B 868 (2025) 139816

Contents lists available at ScienceDirect

Physics Letters B

journal homepage: www.elsevier.com/locate/physletb

Letter

Electron screening in lithium-induced nuclear reactions

A. Cvetinović [a,*], M. Lipoglavšek [a], D. Đukić [b,c], M. Kelemen [a], M. Čekada [a], M. La Cognata [d], S. Markelj [a], S. Palmerini [d,e,f], T. Schwarz-Selinger [g]

[a] Jožef Stefan Institute, Ljubljana, Slovenia
[b] University of Banja Luka, Faculty of Mechanical Engineering, Banja Luka, Bosnia and Herzegovina
[c] Jožef Stefan International Postgraduate School, Ljubljana, Slovenia
[d] INFN-Laboratori Nazionali del Sud, Catania, Italy
[e] Università degli Studi di Perugia, Department of Physics and Geology, Perugia, Italy
[f] INFN-sezione di Perugia, Perugia, Italy
[g] Max-Planck-Institut für Plasmaphysik, Garching, Germany

ARTICLE INFO

Editor: Prof. Betram Blank

Keywords:
Low energy nuclear reactions
Cross section measurements
Electron screening

ABSTRACT

The electron screening effect was studied in the $^{1}H(^{7}Li,\alpha)^{4}He$, $^{2}H(^{6}Li,\alpha)^{4}He$, $^{2}H(^{6}Li,p_0)^{7}Li$ and $^{2}H(^{6}Li,p_1)^{7}Li$ nuclear reactions on thin Ti, thick Pd and thin amorphous carbon targets containing hydrogen and deuterium. In the first three reactions, we measured high electron screening potentials for all targets that are significantly above the theoretical upper limit given by the adiabatic model, but in the last reaction we did not detect any enhancement of the cross section due to electron screening. This is the first time that different screening potentials were measured for the p_0 and p_1 reaction channels.

1. Astrophysical motivation

The study of charged-particle-induced nuclear reactions at astrophysical energies as a means of element production in the universe has been the focus of comprehensive theoretical and experimental research. While the predictions of Standard Big-Bang Nucleosynthesis (SBBN) theory [1,2] and stellar nucleosynthesis can explain the production of nearly all elements of the periodic table, the unresolved "Cosmological Lithium Problem" presents a significant challenge. In particular, the severe discrepancy between SBBN predictions and the abundances of lithium isotopes (^{6}Li and ^{7}Li) observed from metal-poor stars has yet to be resolved [3]. The role of lithium destruction in understanding the abundance problem is undeniable: it may be enhanced by unknown or poorly measured resonances or other unknown effects that increase reaction rates [4]. Moreover, in the context of stellar nucleosynthesis, the $^{7}Li(p,\alpha)^{4}He$ reaction is the final step in the hydrogen-to-helium burning chain [5], contributing to approximately 10 % of the energy budget provided by the whole proton-proton chain [5,6]. To match precise abundance observations with a theory, we need to enhance our understanding of nuclear reaction processes at low energies.

In the case of charged-particle-induced nuclear reactions at energies relevant to astrophysics (well below the Coulomb barrier), the cross section (σ(E)) decreases steeply as the reaction energy (E) decreases. This decrease is due to the strong repulsive Coulomb barrier in the entrance channel, which can only be overcome by the tunneling effects. However, when tunneling through the potential barrier, the probability of the reaction taking place drops sharply as beam energy decreases, making the study of nuclear reactions at astrophysical energies very challenging. Indeed, low energy cross-sections are usually estimated by an extrapolation of the energy dependence of σ(E) measured at higher energies. To simplify extrapolation, the astrophysical $S(E)$ factor is usually introduced:

$$\sigma(E) = \frac{S(E)}{E} e^{-2\pi\eta}. \quad (1)$$

$S(E)$ contains all nuclear effects and, differently from the cross section, in the case of non-resonant reactions varies smoothly with energy [4]. Here E denotes the center-of-mass energy and $\eta(E) = Z_1 Z_2 \alpha(\mu c^2/2E)^{1/2}$ is the Sommerfeld parameter (Z_1 and Z_2 are atomic numbers of the target and projectile, α is the fine structure constant, μ is the reduced mass, and c is the velocity of light). However, a drawback of extrapolation is that it can fail to predict important contributions to the excitation functions such as sub-threshold and low-energy resonances.

In Eq. (1), it is assumed that the Coulomb potential between the target nucleus and the projectile arises from bare nuclei. However, in nuclear reactions induced by charged low-energy particles, atomic electrons can play a role by screening the nuclear charge. Consequently, instead of decreasing with projectile energy as in the case of bare nuclei, due to the presence of electrons the barrier penetrability is constant

* Corresponding author.
E-mail address: aleksandra.cvetinovic@ijs.si (A. Cvetinović).

https://doi.org/10.1016/j.physletb.2025.139816
Received 2 September 2024; Received in revised form 6 August 2025; Accepted 8 August 2025
Available online 11 August 2025

below a certain energy, leading to an increase in the measured cross section at astrophysical energies. This effect is known as electron screening and was anticipated for classical plasmas [7] in the 1950s and experimentally observed 30 years later in nuclear reactions on gaseous targets [8]. Theory provides an upper limit for the electron screening potential (U_e) (the adiabatic limit) for which the reduction of the Coulomb barrier can be estimated as a gain in electron binding energy before and after fusion [9]. However, numerous research groups (see Refs. [10–18] and references therein) have reported values for electron screening potentials significantly higher than the adiabatic limit. The potentials measured in gas targets, where only bound atomic electrons contribute, are consistent with the adiabatic limit [12]. The situation changes, however, for metallic targets, where the main contribution to the screening energy results from quasi-free conduction electrons. Experiments on solid targets have shown that electron screening is particularly strong when light target nuclei are embedded in metals [10–14,16–18]. In these cases, a strong material dependence of screening energies was observed, and values more than one order of magnitude higher than the corresponding adiabatic limit were measured [17,18]. The theoretical approach based on the self-consistent dielectric function theory [15,19], taking into account polarization of free and bound electrons as well as the contribution of cohesion energy may correctly describe high material dependence, but fails by a factor of about three in absolute values of screening energies. Large electron screening was measured for the d + d reaction in different metallic environments [10–12], for experiments with ^{6}Li and ^{7}Li [11,13,20] and for other nuclear reactions [21–23] as well as in experiments employing inverse kinematics [17,18].

This discrepancy might be explained by a series of experiments performed in inverse kinematics [17,18] where it was shown that the presence of specific defects in a crystal lattice, induced by long-term irradiation or mechanical stress of the target, significantly increases the experimental values of the screening potential. These defects predetermine at which position in the crystal lattice of the host material the target nuclei will be trapped. As certain positions in the crystal lattice will have higher densities of valence electrons, this will cause higher electron screening. Accordingly, target nuclei are brought to positions in the crystal lattice with electron densities around the implanted target nuclei that are much higher than those occupied by the target nuclei in regular interstitial positions. An example of this behavior is observed in palladium; when the same target was cold-rolled, it exhibited electron screening several times larger compared to the case when it was annealed [17,18]. An independent study of the d + d reaction [24] showed similar lattice-dependent effects of electron screening potential induced by implanted deuterium and small amounts of oxygen impurities.

Understanding electron screening is very important for nucleosynthesis calculations. Precise reaction rates should be known at very low energies where the contribution of screening effects is significant, and electron screening must be included in most calculations related to the nucleosynthesis of elements. However, this is currently impossible because we lack sufficient knowledge about this effect. A classical theory [25] on electron dynamics, together with the simple view of Ref. [8], as well as different approaches describing weakly and strongly coupled plasmas, taking into account classical and quantum mechanical effects [26] were employed to describe electron screening in plasma. At present, however, there is no existing experimental study of the screening effect in stellar plasmas, though this might be achievable in the future with reaction experiments utilizing high-powered lasers [27,28]. The electron screening effect is especially important for the proton-deuteron-mixture plasma in dense atmospheres of giant planets, brown and white dwarfs, where the reaction rates can increase by many orders of magnitude due to the screening effect [26]. Plasma electrons could be viewed similarly to valence electrons in metals, constantly replacing each other near target nuclei due to their higher mobility. In plasma, the electrons and ions move nearly independent of each other, resulting in many quasi-free electrons. Accordingly, the screening is so large in inverse kinematics because the hydrogen nucleus floats in a sea of valence electrons, coming much closer to the nucleus than its own electron. However, a unified theory of electron screening effects considering collective electron interaction leading to localization of electrons around the crystal vacancies and an increase of its effective masses is still missing. To answer some of these questions, new experiments devoted to study of electron screening in both plasma and solid materials are necessary.

To account for electron screening, the enhancement factor f of the nuclear reaction cross section can be defined as the ratio of the screened (σ_s) and bare-nucleus (σ_b) cross sections [15]:

$$f(U_e) = \frac{\sigma_s}{\sigma_b} = \exp\left[Z_1 Z_2 e^2 / 2\epsilon_0 \hbar \left(\sqrt{\frac{\mu}{2E}} - \sqrt{\frac{\mu}{2(E+U_e)}}\right)\right]. \quad (2)$$

The bare nucleus cross section at astrophysical energies can be measured under certain kinematic conditions by applying indirect methods [29] such as the Trojan Horse Method (THM) (see Spitaleri [30] and the references therein). The THM is based on the Quasi-Free (QF) mechanism reaction theory (see, [34] and references therein) and allows measurement of bare nucleus cross sections inside the Gamow energy window without the difficulties related to Coulomb barrier suppression or electron screening contribution to the cross section. However, indirect methods can only be applied to a limited number of cases.

We recently achieved interesting results in an electron screening study in the ^{7}Li + p and ^{6}Li + d nuclear reactions with H and D implanted in different targets.

2. Experimental setup and target preparation

The experimental study of the electron screening effect was performed in inverse kinematics using the 2 MV Tandetron accelerator at the Microanalytical Center of Jožef Stefan Institute (JSI) by measuring the rates of the following nuclear reactions:

$$\begin{aligned} &^7\mathrm{Li} + \mathrm{p} \rightarrow {}^8\mathrm{Be}^* \rightarrow {}^4\mathrm{He} + {}^4\mathrm{He}, \\ &^6\mathrm{Li} + \mathrm{d} \rightarrow {}^8\mathrm{Be}^* \rightarrow {}^4\mathrm{He} + {}^4\mathrm{He}, \rightarrow {}^7\mathrm{Li} + \mathrm{p}_0, \rightarrow {}^7\mathrm{Li}^* + \mathrm{p}_1, \end{aligned} \quad (3)$$

on thin titanium and two differently prepared thick palladium targets containing hydrogen and deuterium, and thin amorphous carbon targets containing hydrogen (aCH) and deuterium (aCD).

Protons and α particles emitted from the reactions were detected by a 300 μm thick silicon detector with an active area of 50 mm^2, placed 32 mm from the target at an angle of 135° compared to the direction of the lithium ion beams (see the scheme in Fig. 1). The detector was calibrated using an ^{241}Am α-particle source, and we obtained a geometric efficiency of 0.00478. The energy resolution of the detection system was 28 keV for α particles. In order to prevent scattered beam particles from hitting the detector, an 8 μm thick Al absorber was placed in front of the silicon detector. The electronic threshold was set at 50 keV.

The reaction induced with ^{7}Li was measured in an energy region between 0.439 and 2.063 MeV, while the energy of the ^{6}Li beam was in the range between 0.331 and 3.072 MeV. The beam currents were between 0.3 and 10 μA, depending on the beam energy. The numbers of incident ions were deduced by measuring the charge collected in the

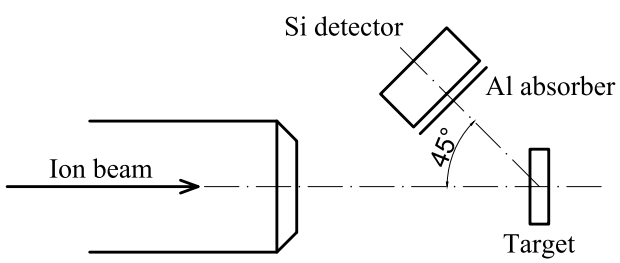

Fig. 1. The scheme of the experimental setup used for the experiments performed in inverse kinematics.

electrically isolated target chamber. To correct the detected yields for the α-particle background present in the laboratory, background spectra were recorded for several days without beam.

For our study of electron screening, we chose Ti, Pd and C as hosting materials as these materials have the ability to absorb large volumetric quantities of hydrogen. The Ti target was a 110 nm thick Ti layer deposited by sputtering on a Ta backing and then implanted with hydrogen or deuterium (H/D) using a Tectra IonEtch ion gun. The foil was bombarded for about 24 h with the hydrogen or deuterium beam accelerated by an extraction voltage of 3.5 kV. The beam current was 200 μA, and was wide enough that the implantation spot size covered the whole target. During implantation, the target was mounted on a 10 cm long copper holder with a diameter of 5 cm for passive cooling, which effectively prevented substantial heating of the foil. In spite of the fact that proton range at 3.5 keV is 41 nm [31] in Ti, due to hydrogen diffusion, the foil had a uniform hydrogen concentration through its whole thickness (see Fig. 2).

Two 2.5x2.5 cm^2 palladium targets were used. The first target was Chempur's 100 μm thick palladium foil (Soft Pd) and the second was a 100 μm thick cold rolled palladium foil (Hard Pd) produced according to our specifications, at Zlatarna Celje. It was cold rolled from a thickness of about 2.5 mm to 0.1 mm. This foil was much less flexible than the first target. The purities of both were above 99.9 %, and to prepare the targets for electron screening studies, samples were loaded with H/D by leaving them in the corresponding gas at the pressure of 1 bar and the temperature of 24 °C for 24 hours.

The hydrogen gas used for the Ti and Pd target loading was natural, however, deuterium gas was a mixture containing 85 at. % deuterium and 15 % hydrogen.

The last two targets were H/D-containing targets consisting of dense, plasma-deposited thin amorphous hydrocarbon (aCH) and deuterated hydrocarbon (aCD) films grown on a single crystal silicon (100) substrate [32]. The thickness of the aCH target was 60 nm and of aCD was 275 nm, as measured with tactile profilometry. The H/D amount relative to the number of C atoms was about 52 % with a total relative uncertainty of 10 % [32].

To determine the deuterium depth distribution, we performed quantitative deuterium depth profiling with the Nuclear Reaction Analysis (NRA) technique for each target. For this purpose, high-energy protons emitted in the ^{2}H(^{3}He,p)^{4}He reaction were measured at six ^{3}He energies, in an energy range from 0.629 to 4.297 MeV. The deuterium depth profiles were obtained by fitting the NRA spectra using the SIMNRA code [33]. Fig. 2 shows deuterium depth distributions measured in our targets.

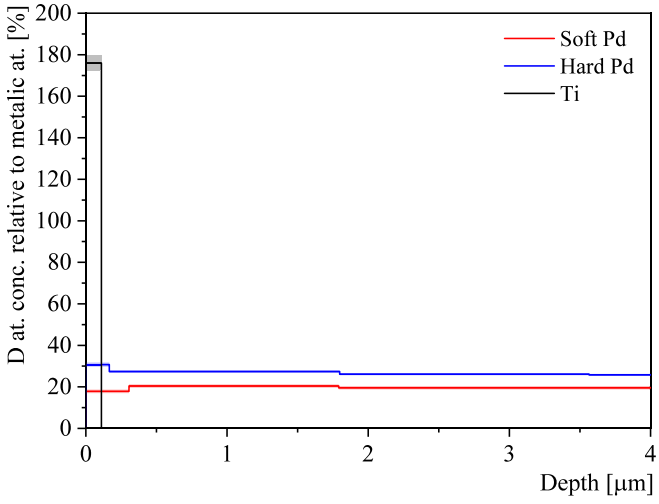

Fig. 2. Deuterium concentration relative to palladium and titanium as a function of depth in the target, measured in Soft Pd (red line), Hard Pd (blue line) and thin titanium targets using the Nuclear Reaction Analysis technique recorded after the samples were bombarded with an energetic Li ion beam for several hours causing H/D evaporation. Shaded areas represent errors to the fitted deuterium concentrations obtained using SIMNRA code [33].

A uniform deuterium depth distribution was found in all targets even after the samples were bombarded with an energetic Li ion beam causing H/D evaporation (see Fig. 2). Since we do not expect the two hydrogen isotopes to behave differently, we assumed a uniform depth distribution for protons, as well. In the Ti target we measured a maximum concentration of H/D relative to the number of metallic atoms of 200 % with an uncertainty of 4 % as estimated with SIMNRA [33]. Although both of our Pd targets had uniform D distribution and were loaded with H/D at the same time in the same gas chamber, in the Soft Pd foil maximum concentrations of 70 % of H/D per metallic atom were achieved. This is consistent with the limit of hydrogen absorption at normal pressures [34] when approximately 70 % of the octahedral holes are occupied. However, the cold-rolled (Hard Pd) foil could be loaded only up to 47 % of H/D per metallic atom as determined gravimetrically. Uncertainties of hydrogen concentration were less than 0.5 %.

To effectively prevent substantial heating of the targets during the experiment, samples were mounted on a 5x5 cm and 1 cm thick copper holder. Targets were positioned in a high vacuum chamber perpendicularly to the beam direction. During the experiment, we monitored hydrogen and deuterium loss in all targets by repeatedly measuring the yields at the beam energies of 2.063 and 3.072 MeV for the ^{7}Li + p and ^{6}Li + d reactions, respectively, before and after each measurement at other energies. The highest hydrogen loss was obtained in the Hard Pd target, typically of about 18 % between the first and last control measurements, and the smallest, of about 6 %, was found in aCH and aCD targets. To correct for the H/D loss, we normalized the detected yields for a given beam energy to the average of the two control measurements.

3. Electron screening in the ^{7}Li + p→2α and ^{6}Li + d→2α reactions

According to the definition of the cross section σ in the case of a thin target [35], the experimentally measured α-particle yield N_α is defined by the equation:

$$N_\alpha = 2\epsilon\sigma W_\alpha N_{Li} n \frac{\rho N_A x}{M}, \tag{4}$$

where ϵ is the efficiency of the detector, W_α is the angular distribution factor for emitted α particles, N_{Li} is the number of incident Li ions and the value $n\frac{\rho N_A d}{M}$ represents the surface density of H/D atoms in the target (n being the number of H/D atoms per crystal lattice atom, x the target thickness, N_A, ρ and M the Avogadro's number, target density and molar mass, respectively). The factor of 2 in this equation takes into account two identical α particles emitted in the observed reaction.

Since the ^{7}Li + p and ^{6}Li + d reactions do not have any known resonances in the studied lithium energy range, the α-particle yield for thick targets with a homogeneous distribution of hydrogen, has to be calculated by transforming Eq. (4) into a differential form and integrating over energies from the beam energy E_0 to 0:

$$N_\alpha = N_{Li} n \frac{\rho N_A}{M} \int_{E_0}^{0} \epsilon W_\alpha \frac{\sigma_E}{dE_{Li}/dx} dE_{Li}. \tag{5}$$

The stopping power dE_{Li}/dx was calculated using the SRIM code [31] and the angular distributions were taken from [36].

The detected number of α particles N_α was deduced by subtracting the background from recorded spectra and counting the number of α particles in the correct energy window for each beam energy. This was possible due to the simplicity of the spectra, reflected in the fact that background radiation and noise were low in a wide energy window around the energies corresponding to α particles from the studied reactions. The target thickness was divided into many thin layers for which the energy loss (ΔE) is negligible compared to the beam energy, and the

cross section was calculated for each of these layers. An example of the recorded spectrum showing peaks of α-particles and protons (p_0 and p_1) coming from the ^{2}H(^{6}Li,α)^{4}He, ^{2}H(^{6}Li,p_0)^{7}Li and ^{2}H(^{6}Li,p_1)^{7}Li reaction channels, respectively, is shown in Fig. 3.

To determine the electron screening potential, according to Eq. (2), first we calculated the enhancement factors by dividing our experimentally deduced screened-nucleus S-factors with the bare-nucleus S-factors determined using the THM [30] from Lamia [6] for the ^{1}H(^{7}Li,α)^{4}He nuclear reaction and from Spitaleri [37] for the ^{2}H(^{6}Li,α)^{4}He reaction. The enhancement factors were then fitted by Eq. (2) with the electron screening potential U_e left as the only free parameter. Resulting from the one-parameter least-squares fit to the data we obtained, the screening potentials listed in Table 1. Fig. 4 shows the integrated enhancement factor for the ^{1}H(^{7}Li,α)^{4}He reaction as a function of center-of-mass energy E in our targets. The integrated enhancement factor for the ^{2}H(^{6}Li,α)^{4}He reaction as a function of E is shown in Fig. 5. Surprisingly, much larger electron screening was measured for the ^{2}H(^{6}Li,α)^{4}He reaction than in the ^{1}H(^{7}Li,α)^{4}He reaction in all three targets, showing isotopic dependence of the screening potential for many of the targets. However, we did not notice such dependence in previous experiments, where we studied the ^{19}F + ^{1}H and ^{19}F + ^{2}H nuclear reactions in H/D containing palladium targets with the ^{19}F beam [18]. The reason for this difference may be due to the use of the overly simplified Gamow factor for barrier penetration in the case of the ^{6}Li + ^{2}H reaction. As seen in Fig. 6, the bare-nucleus astrophysical S-factor increases towards lower energies, meaning that the barrier penetration probability is higher than the Gamow factor predictions. On top of that, we apply the screening potential that enhances the error in barrier penetration. The ^{6}Li + d reaction has not been studied before in electron screening studies, so it might be that this is a special reaction, possibly due to the cluster structure of ^{6}Li, which is composed of a tightly bound alpha particle and a deuteron. It is possible that some reorientation might occur before the reaction at low energies, and that this effect is more pronounced in the presence of electrons.

The comparison of the bare-nucleus astrophysical S-factor determined by the THM [37] with the screened-nucleus astrophysical S-factor measured in this study with the amorphous carbon target containing deuterium is shown in Fig. 6. The difference between the THM and our experimental S-factor is as expected. At high energies the electron screening has little influence and the two S-factors agree with each other, while at lower energies the screening-influenced experimental S-factor gradually becomes much larger than the THM one.

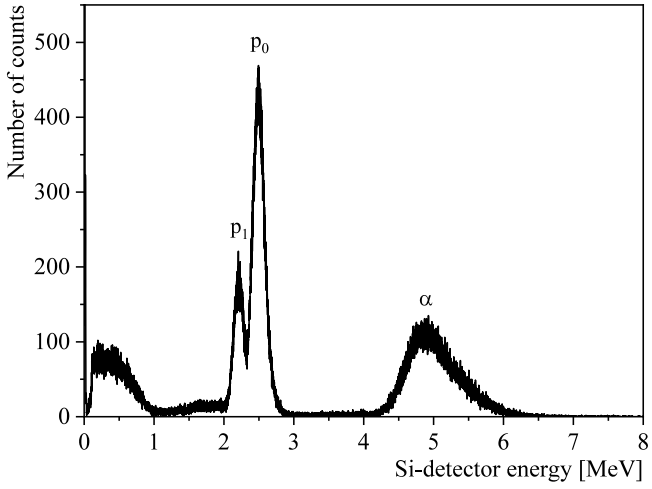

Fig. 3. The spectrum obtained in the silicon detector for the Hard Pd target at ^{6}Li beam energy of 2.057 MeV. Peaks corresponding to α particles and protons (p_0 and p_1) coming from the ^{2}H(^{6}Li,α)^{4}He, ^{2}H(^{6}Li,p_0)^{7}Li and ^{2}H(^{6}Li,p_1)^{7}Li reaction channels, respectively, can be seen clearly.

Table 1
The electron screening potentials U_e measured in the ^{1}H(^{7}Li,α)^{4}He, ^{2}H(^{6}Li,α)^{4}He and ^{2}H(^{6}Li,p_0)^{7}Li reactions in the Ti, Hard Pd, Soft Pd, aCH and aCD targets. The predicted upper limit for the screening potential given by the adiabatic model is 0.24 keV for all reactions.

Reaction	U_e [keV]			
	Ti	Hard Pd	Soft Pd	aCH/aCD
^{1}H(^{7}Li,α)^{4}He	1.7 ± 0.8	2.8 ± 1.0	≤ 1.4	3.2 ± 1.5
^{2}H(^{6}Li,α)^{4}He	11.0 ± 2.1	8.4 ± 1.2	5.2 ± 1.4	13.1 ± 1.9
^{2}H(^{6}Li,p_0)^{7}Li	11.0 ± 3.4	12.2 ± 1.5	–	17.2 ± 4.0

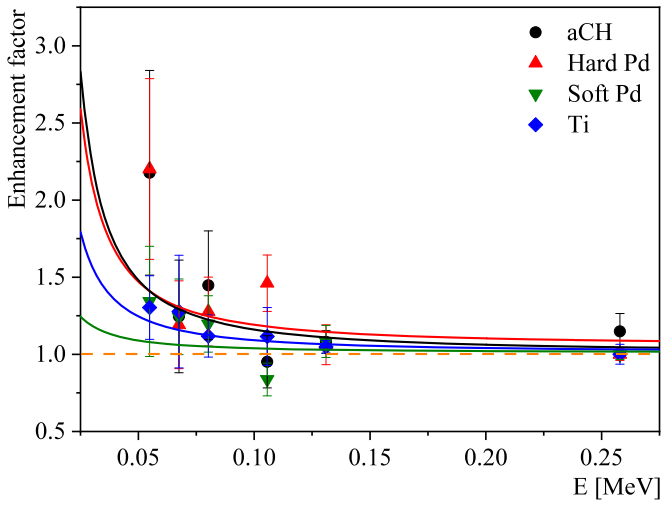

Fig. 4. The integrated enhancement factor as a function of the center-of-mass energy for the ^{1}H(^{7}Li,α)^{4}He reaction in the Ti (blue rhombus), Hard Pd (red up-pointing triangles), Soft Pd (green down-pointing triangles) and aCH (black circles) targets. Points represent the experimental data and solid lines represent least-squares fits using Eq. (2). Dashed orange line represents no-enhancement-baseline, when $U_e = 0$.

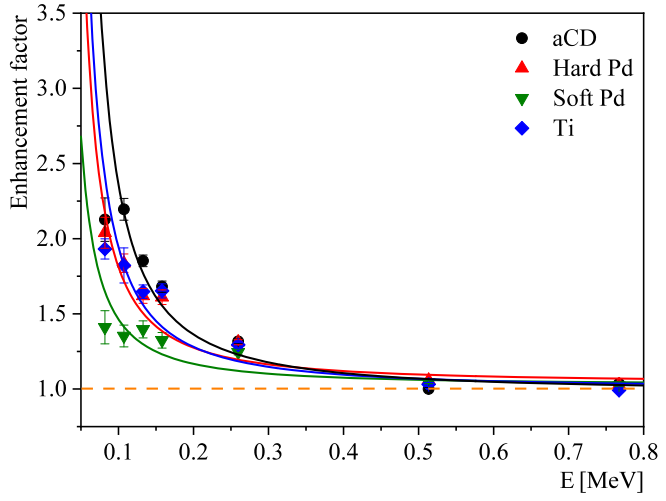

Fig. 5. The integrated enhancement factor as a function of the center-of-mass energy for the ^{2}H(^{6}Li,α)^{4}He reaction in the Ti (blue rhombus), Hard Pd (red up-pointing triangles), Soft Pd (green down-pointing triangles) and aCD (black circles) targets. Points represent the experimental data and solid lines represent least-squares fits using Eq. (2). Dashed orange line represents no-enhancement-baseline, when $U_e = 0$.

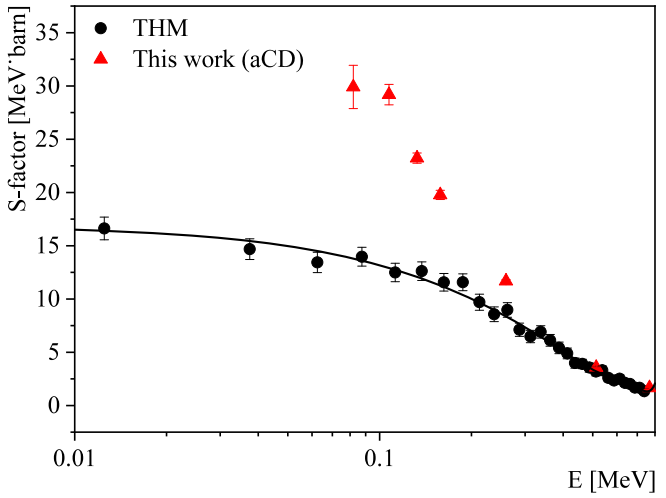

Fig. 6. The astrophysical *S*-factors as a function of the center-of-mass energy for the ^{2}H(^{6}Li,α)^{4}He reaction. The black points and black solid line represent the bare-nucleus astrophysical *S*-factor, which is not affected by the screening effect and was determined by the Trojan Horse method [37]. The red triangles represent the screened-nucleus astrophysical *S*-factor measured in this study with the amorphous carbon target containing deuterium. The difference between the two data sets is due to the screening effect influencing our data.

4. Electron screening in the ^{6}Li + d→^{7}Li + p_0 and ^{6}Li + d→^{7}Li + p_1 channels

The detected numbers of protons from the p_0 and p_1 channels N_p was deduced by fitting the corresponding peak in recorded spectra with Gaussian shape, and the background in the spectra was subtracted by a linear function, including a step function. An example of the recorded spectrum is shown in Fig. 3.

The electron screening potential was calculated similarly as for the nuclear reaction with two α particles in the exit channel. We tried to calculate the enhancement factors by taking the cross sections from Elwyn [38]. However, the astrophysical *S*-factors determined from our experimental data did not agree well with the *S*-factors in Elwyn [38] for both channels. Namely, the two data sets did not follow the same trend and our points toward lower energies were below the points from Elwyn [38]. As a result, we deduced the bare-nucleus astrophysical *S*-factors for two channels assuming that the screening potential for the p_0 reaction channel in our Soft Pd target is the same as measured in the reaction with two α-particles in the exit channel, as in this target we measured the smallest screening potential. In this manner the procedure would introduce the smallest error in the case that a wrong value for the screening potential is assumed. By fitting $U_e = 5.2$ keV in Soft Pd, we deduced the bare-nucleus astrophysical *S*-factor:

$$S(E) = 24.45 - 34.54E + 18.04E^2 [MeVb] \quad (6)$$

for the ^{2}H(^{6}Li,p_0)^{7}Li reaction channel with normalization.

This result for the bare-nucleus astrophysical *S*-factor also perfectly fit our experimental data for the astrophysical *S*-factor of ^{2}H(^{6}Li,p_1)^{7}Li reaction channel in the same target, so we assume no electron screening in Soft Pd for the p_1 channel. Eq. 6 was then used to calculate the enhancement factors by dividing our experimentally deduced screened S-factors for both reaction channels in all targets. The screening potentials resulting from the one-parameter least-squares fit to the experimental enhancement factors fit by Eq. (2) with the electron screening potential U_e left as the only free parameter, are listed in Table 1). Fig. 7 shows the integrated enhancement factor for the ^{2}H(^{6}Li,p_0)^{7}Li and ^{2}H(^{6}Li,p_1)^{7}Li reaction channels as a function of E in Ti, Hard Pd and aCD targets.

Large electron screening was measured in all four targets for the ^{2}H(^{6}Li,p_0)^{7}Li reaction channel (see Table 1). However, the results

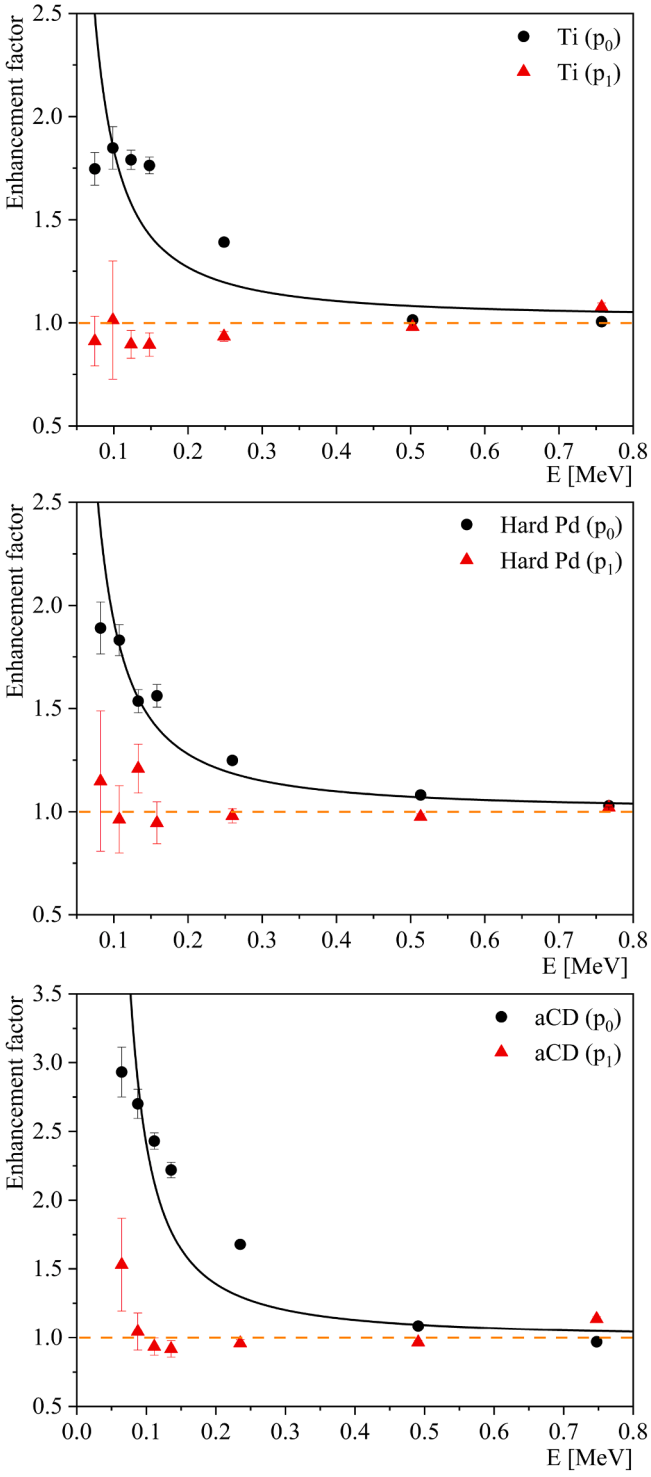

Fig. 7. The integrated enhancement factor as a function of the center-of-mass energy for the ^{2}H(^{6}Li,p_0)^{7}Li and ^{2}H(^{6}Li,p_1)^{7}Li* reaction channels in the Ti, Hard Pd and aCD targets. Points represent the experimental data and solid lines are least-squares fits using Eq. (2). Dashed orange line represents no-enhancement-baseline, when $U_e = 0$.

showed no electron screening for the ^{2}H(^{6}Li,p_1)^{7}Li channel. This cannot be explained by the static picture of electron screening given by the adiabatic model, but could be interpreted by understanding the details of the reaction mechanism: the spins and parities of both particles in the entrance channel, ^{6}Li and ^{2}H, are $J^{\pi} = 1^{+}$. The ground state of ^{7}Li has $J^{\pi} = 3/2^{-}$, meaning that the proton p_0 has to carry away no orbital angular momentum. When leaving the compound nucleus ^{8}Be, it only has

to cross the Coulomb barrier, which in this case amounts to 1.9 MeV. The Q-value of the reaction is 5 MeV and the excitation energy lifts p_0 above the Coulomb barrier, making it free to leave the compound nucleus. However, the situation is different in the case of the ^{2}H(^{6}Li,p_1)^{7}Li reaction channel. The first excited state of ^{7}Li has spin $J^\pi = 1/2^-$ meaning that the proton p_1 has to carry away one unit of angular momentum. The combined Coulomb and centrifugal barriers are more than 10 MeV in this case, meaning that the proton p_1 has to tunnel through the barrier like in the entrance channel. However, the electron that screened the barrier in the entrance channel is now gone, and the barrier in the exit channel is not screened - hence, there is no enhancement of this exit channel at low beam energies.

5. Conclusions

The electron screening effect was studied in the ^{1}H(^{7}Li,α)^{4}He, ^{2}H(^{6}Li,α)^{4}He, ^{2}H(^{6}Li,p_0)^{7}Li and ^{2}H(^{6}Li,p_1)^{7}Li nuclear reactions on thin Ti, thick Pd and thin amorphous carbon targets containing hydrogen and deuterium. In the first three reactions we measured high electron screening potentials for all targets that are significantly above the theoretical upper limit given by the adiabatic model, but in the last reaction we did not detect any enhancement of the cross section due to electron screening above the adiabatic limit, respecting statistical uncertainties. This is the first time that different screening potentials were measured for the p_0 and p_1 reaction channels and sheds new light on the long-standing electron screening problem. With the ^{6}Li ion beam we measured much larger electron screening than with ^{7}Li in all targets. However, an isotopic dependence was not observed in previous experiments where we studied the ^{19}F + ^{1}H and ^{19}F + ^{2}H nuclear reactions [18] in H/D containing palladium targets with the ^{19}F beam. This could indicate a wrong penetration factor for the ^{2}H + ^{6}Li nuclear reaction; the bare-nucleus astrophysical *S*-factor increases towards lower energies, meaning that the barrier penetration probability is higher than the Gamow factor predictions (additionally we applied the screening potential that enhances the error in barrier penetration). The ^{6}Li + d reaction has not been studied before in electron screening studies. It could be that this is a special reaction, possibly due to the cluster structure of ^{6}Li, which is composed of a tightly bound alpha particle and a deuteron. Possibly some reorientation might occur before the reaction at low energies, and that this effect is more pronounced in the presence of electrons.

Our results clearly show that the large screening effect cannot be caused by the static electron densities around interacting nuclei, since this approach can only describe small electron screenings obtained in gases or virgin solid targets. Our results show the necessity of adopting a new approach for electron screening calculations considering a collective electron interaction leading to localization of electrons around the crystal vacancies and an increase of its effective masses.

It is recommended to perform new measurements to investigate this newly discovered dependence of screening energies on reaction channels.

Data availability

Data will be made available on request.

Declaration of competing interest

The authors declare that they have no known competing financial interests or personal relationships that could have appeared to influence the work reported in this paper.

Acknowledgements

This work was partially supported by the Horizon2020 Framework Programme under the grant “Clean Energy from Hydrogen-Metal Systems” (951974).

References

[1] B.D. Fields, Ann. Rev. Nucl. Part. Sci. 61:47 (2011).
[2] A. Coc, et al., Astrophys. J. 600 (2004) 544.
[3] L. Sbordone, et al., A A 522 (2010) A26.
[4] C. Iliadis, Nuclear Physics of Stars - Second, Revised and Enlarged Edition Wiley-VCH, Weinheim (2015).
[5] H. Spinka, et al., Nuc. Phys. A 164 (1971) 1.
[6] L. Lamia, et al., Astron. Astrophys. 541 (2012) A158.
[7] E.E. Salpeter, Austr. J. Phys. 7 (1954) 373.
[8] H.J. Assenbaum, et al., Z. Phys. A: At. Nucl. 327 (1987) 461.
[9] F. Strieder, et al., Nature 88 (2001) 461.
[10] K. Czerski, et al., Europhys. Lett. 68 (2004) 363.
[11] J. Kasagi, et al., J. Phys. Soc. Jpn. 73 (2004) 608.
[12] F. Raiola, et al., J. Phys. G 31 (2005) 1141.
[13] J. Cruz, et al., Phys. Lett. B 624 (2005) 181.
[14] T.S. Wang, et al., J. Phys. G: Nucl. Part. Phys. 34 (2007) 2255.
[15] A. Huke, et al., Phys. Rev. C 78 (2008) 015803.
[16] M. Lipoglavšek, et al., Eur. Phys. J. A 44 (2010) 71.
[17] A. Cvetinović, et al., Phys. Rev. C 92 (2015) 065801.
[18] A. Cvetinović, et al., Phys. Lett. B 838 (2023) 137684.
[19] K. Czerski, et al., Europhys. Lett. 113 (2016) 22001.
[20] J. Cruz, et al., J. Phys. G: Nucl. Part. Phys. 35 (2008) 014004.
[21] K.U. Kettner, et al., Atom. Nucl. 298 (1980) 65.
[22] C. Rolfs, et al., Nucl. Instr. and Meth. Phys. Res. B 99 (1995) 297.
[23] T.S. Wang, et al., Eur. Phys. J. A 28 (2006) 375.
[24] A. Kowalska, et al., Mater. (Basel) 16 (2023) 6255.
[25] C. Rolfs, Prog. Theor. Phys. Supl. 154 (2004) 373.
[26] S. Ichimaru, H. Kitamura, Phys. Plasma. 6 (1999) 2649.
[27] D.T. Casey, et al., Front. Phys. 10 (2023).
[28] D. Mascali, et al., Universe 8(2) (2022) 80.
[29] R.E. Tribble, et al., Rep. Prog. Phys 77 (2014) 106901.
[30] C. Spitaleri, et al., Eur. Phys. J. A 55 (2019) 161.
[31] J.F. Ziegler, et al., The Stopping and Range of Ions in Matter Lulu Press Co., Morrisville, NC), https://www.srim.org (2008).
[32] T. Schwarz-Selinger, et al., J. Appl. Phys. 86 (1999) 3988.
[33] M. Mayer, SIMNRA User’s Guide, Report IPP 9/113, Max-Planck-Institut für Plasmaphysik, Garching, Germany, (1997) https://mam.home.ipp.mpg.de.
[34] G. Alefeld, J. Völkl, Hydrogen in Metals II, Application-Oriented Properties 29 (1978) p. 81.
[35] C. Rolfs, R.W. Kavanagh, Nucl. Phys. A 455 (1986) 179.
[36] S. Engstler, et al., Z. Phys. A: Hadrons Nucl. 342 (1992) 471.
[37] C. Spitaleri, et al., Phys. Rev., C 63 (2001) 055801.
[38] A.J. Elwyn, et al., Phys. Rev. C 16 (1977) 1744.